EES Catalysis

PAPER

View Article Online
View Journal



Cite this: DOI: 10.1039/d6ey00038j

# Mechanism study on hydrogen generation from metal hydride-coupled methanol steam reforming

Kuerbangnisha Kadeer,[a] Yufei Jiang,[a] Xiao Liu,[b] Tingzhou Li,[a] Guofu Lu,[a] Chaoyuan Hu,[a] Yu Shi,[b] Xingguo Li,[a] Fangqin Guo,[c] Takayuki Ichikawa,[c] Lei Xie*[b] and Jie Zheng*[a]

Received 24th February 2026,
Accepted 29th March 2026

DOI: 10.1039/d6ey00038j

rsc.li/eescatalysis

Metal hydride (MH)-coupled methanol steam reforming (MSR), in which MSR is coupled with the hydrolysis of MH, is an attractive strategy for onsite hydrogen generation as it offers a high hydrogen density, high hydrogen purity and balanced thermal effect. This study provides a comprehensive mechanism study on the MH-coupled MSR over Cu/$CaH_2$ using online mass spectroscopy coupled with isotope labelling and *in situ* Fourier-transformed infrared spectroscopy. Results show that the hydrolysis of MH and MSR over Cu proceeds simultaneously *via* a formate-mediated pathway. The stepwise dehydrogenation of methanol primarily occurs on the Cu surface, while $CaH_2$ effectively activates $CH_3OH$ at low temperatures by supplying the hydrolysis heat to the endothermic MSR. Although $Ca(OCH_3)_2$ and $Ca(HCOO)_2$ can be formed when $CaH_2$ is introduced, they are not active intermediates in the MH-coupled MSR due to their high thermal stability. Instead, they are converted back to $CH_3OH$ and HCOOH *via* hydrolysis.

**Broader context**

Hydrogen is a key vector for decarbonizing energy systems, yet efficient and high-purity on-demand hydrogen production remains challenging. Methanol steam reforming (MSR) is attractive due to its high hydrogen density and the handling advantages of a liquid carrier but its intrinsic endothermicity and CO formation limit its practical application. Meanwhile, metal hydrides (MHs) have been extensively studied for their hydrogen production ability, and their potential to participate in hydrogen transfer reactions has recently attracted increasing attention.

In this work, MSR is coupled with metal hydride hydrolysis, where $CaH_2$ acts simultaneously as a catalyst support and as a reactive component. During hydrolysis, $CaH_2$ releases heat and hydrogen and captures $CO_2$, which helps in supplying the heat for MSR and shifts the reaction equilibrium. This coupling not only improves hydrogen production performance but also changes the reaction environment and possible pathways. This work also provides insights into $CO_2$ capture and may inspire new strategies to further enhance the hydrogen storage density of existing hydrogen storage materials.

## 1. Introduction

Hydrogen is the ideal energy source to achieve carbon neutrality due to its high abundance, zero emissions, high efficiency, and renewability.[1–3] The development of high-performance hydrogen storage technologies is crucial for its practical utilization.[4–6] Among the chemical hydrogen production methods, methanol steam reforming (MSR) and metal hydride hydrolysis are promising strategies for hydrogen generation for fuel cells though each presents inherent limitations.[7–9] MSR offers a high hydrogen density (12 wt%) and low cost, but its application hindered is by its endothermic nature and the formation of CO as a byproduct. For MSR, most of the researches have predominantly focused on the rational design of efficient and stable catalysts, achieving significant progress in both activity and durability. For instance, Hu *et al.*[10] developed a highly dispersed Ni-based catalyst supported on spongy mesoporous alumina, which enabled rapid reactant adsorption and efficient methanol dehydrogenation, delivering a high hydrogen yield and excellent long-term stability (12 h). Similarly, Shu *et al.*[11] reported an Ru-based carbon-coated $CeO_2$ catalyst, where the synergistic interaction between the carbon layer and $CeO_2$ enhanced metal–support interactions, facilitated electron transfer, and generated abundant oxygen vacancies, leading to

[a] *Beijing National Laboratory for Molecular Sciences (BNLMS), College of Chemistry and Molecular Engineering, Peking University, Beijing, 100871, China. E-mail: zhengjie@pku.edu.cn*
[b] *Sunan Institute for Molecular Engineering, Peking University, Building 6, Xianshi Road No. 88, Changshu Hi-Tech Industrial Development Zone, Jiangsu, 215500, China. E-mail: xielei@pkusim.com*
[c] *Graduate School of Advanced Science and Engineering, Hiroshima University, Higashihiroshima, 739-8527, Japan*

improved stability and resistance to carbon deposition. Beyond activity and stability, considerable efforts have been devoted to suppressing CO formation.[12–14] At the catalyst level, extensive research has been devoted to the design of highly selective catalysts.[15–17] For example, Xie *et al.*[18] demonstrated that the rod-shaped $CeO_2$ supports enriched oxygen vacancies, promoting both methanol activation and the water–gas shift reaction, thereby reducing CO selectivity. At the system level, new MSR technologies such as absorption-enhanced MSR and electrochemical-assisted MSR[19,20] have been widely developed to enhance hydrogen purity. However, the intrinsic endothermicity remains one of the key challenges in its practical application for onsite hydrogen generation.

Copper-based catalysts are the most widely used MSR catalysts. The reaction mechanism of the MSR over copper-based catalysts has been extensively studied.[21–25] It generally follows two main pathways: the methanol decomposition–water gas shift (MD–WGS) route and the MSR–reverse water gas shift (MSR–rWGS) route.[26] The dominant pathway depends on the type of intermediate formed on the metal surface.[27] When methanol is adsorbed in a bidentate mode *via* both carbon and oxygen atoms ($\eta^2$(C,O)), it tends to decompose into CO and $H_2$. In contrast, monodentate adsorption *via* the oxygen atom ($\eta^1$(O)) leads to intermediates, such as $HCOOCH_3$ or HCOOH, which eventually desorb as $CO_2$ and $H_2$ without forming CO.[28] The metal–support interaction strongly affects the reaction intermediates and plays a crucial role in MSR catalysis.[29–31] Li *et al.*[22] enhanced the performance of a commercial Cu/ZnO/$Al_2O_3$ catalyst by optimizing the activation process, in which the migration of $ZnO_x$ to the Cu surface increased the Cu–$ZnO_x$ interfacial sites and enhanced catalytic activity and stability. Similarly, Franco *et al.*[32] reported that the partial oxidation of $Cu^0$ to $Cu^{\delta+}$ by $CeO_2$ in a CuO/$CeO_2$ catalyst provided active sites for the MSR, while the excellent oxygen storage capacity of $CeO_2$ facilitated oxygen transfer and enhanced $CO_2$ selectivity.

In our previous study, we used $CaH_2$ as the support for Cu catalysts in MSR and demonstrated a new metal hydride (MH)-coupled MSR protocol, in which MSR was coupled with the hydrolysis of MHs.[33,34] The exothermic hydrolysis of metal hydrides supplies heat for the endothermic MSR, and the $CO_2$ generated from the MSR is captured by hydroxides derived from hydride hydrolysis, thereby shifting the equilibrium and suppressing CO formation. Although similar strategies, such as sorption-enhanced MSR,[19] can also achieve high hydrogen purity (up to 99.6%) by introducing $CO_2$ absorbents, they are limited by the reduced hydrogen density, challenges in sorbent regeneration, and lack of thermal integration. In contrast, the MH-coupled MSR system intrinsically integrates heat supply and *in situ* $CO_2$ capture within a single material platform. As a result, it delivers superior hydrogen production performance, including a higher hydrogen density (6.56 wt%) than standalone hydride hydrolysis (5.1 wt% for $CaH_2$ hydrolysis),[35] near-100% hydrogen purity compared to ~75% in conventional MSR,[7] and a more balanced heat profile than MSR, metal hydride hydrolysis, or sorption-enhanced MSR. Beyond the improved reaction performance, from a practical perspective, the coupled system generates a solid product ($Cu/CaCO_3$), implying that the catalyst is not regenerated *in situ*. However, Cu can be recovered from the product using appropriate chelating reagents, and the remaining $CaCO_3$, due to the abundance of calcium, can be disposed of following established procedures or potentially reused as a Ca-based material.

MHs have been increasingly employed as active catalytic components in various hydrogen-involved reactions, such as reversible hydrogen storage in liquid organic hydrogen carriers (LOHCs), $CO_2$ hydrogenation, and chemical looping ammonia synthesis.[36,37] For example, in LOHC dehydrogenation, hydrogen vacancies in MHs facilitate hydrogen release and accelerate the rate-limiting step.[38] In $CO_2$ hydrogenation, MHs act as supplementary hydrogen sources, enhancing the $C_{2+}$ product selectivity under lower $H_2/CO_2$ ratios.[39] In ammonia synthesis, MHs enable milder reaction conditions by preventing hydrogen over-adsorption on transition metals and promoting $N_2$ activation through their electron-donating properties.[40] In these successful examples, the reversible hydrogen absorption and desorption properties of MHs introduce novel hydrogen transfer pathways and active sites, thereby leading to new mechanisms.

Compared to previously reported MH-based catalysis, MH-coupled MSR over $Cu/CaH_2$ exhibits distinct features. Notably, $CaH_2$ functions not only as a support for Cu but also as a hydrogen source *via* hydrolysis, dynamically transforming into hydroxide, accompanied by heat release. In addition, $CaH_2$ may directly react with methanol and intermediates such as HCOOH, potentially introducing alternative reaction pathways. To uncover the underlying mechanism, this study explores potential intermediates and pathways using online mass spectrometry (MS), isotope tracing, *in situ* DRIFTS and other comparative experiments, ultimately proposing a detailed reaction mechanism for the coupled system.

## 2. Experimental

### 2.1 Preparation and characterization of the samples

The $Cu/CaH_2$, $Cu/Ca(OH)_2$ and $Cu/Al_2O_3$ samples were prepared using the methods described in our previous study.[34] Briefly, Cu precursors were mixed with the support *via* either mechanical milling or impregnation, followed by reduction in $Ar/H_2$ flow to yield the corresponding catalysts. All the catalysts contain about 9 wt% Cu. Structural characterizations by XRD and XPS suggest that Cu is mainly in the metallic state, and the supports are generally unaffected.

### 2.2 *In situ* detection of hydrogen evolution by online MS

The online mass spectrometry in this study was conducted using the setup shown in Fig. S1a in the SI. During the test, $CH_3OH$ and $H_2O$ were pumped into the evaporation chamber, and their molar ratios were controlled by adjusting the pumping rates, which were previously calibrated. The $CH_3OH$–$H_2O$ mixture was then vaporized in the evaporation chamber and carried by Ar gas into the reactor containing the catalysts to initiate the hydrogen generation reaction. The evolved gas

products were continuously monitored online using a residual gas analyzer (Pfeiffer Vacuum OmniStar GSD 320) in the scanning mode, covering an $m/z$ range of 0–59. The major gaseous products and their corresponding $m/z$ values in the MS were 2 ($H_2$), 3 (HD), 4 ($D_2$), 18 ($H_2O$), 28 (CO) and 44 ($CO_2$). All signals are calibrated relative to the Ar signal ($m/z$ = 40), which flows at a constant rate of 10 standard cubic centimeters per minute (sccm). To avoid air exposure during the reaction, solid sample loading was carried out inside an Ar-filled glove box. The valves and bypass lines were designed to ensure no air intrusion during system installation.

### 2.3 Isotope tracing experiment

Isotope tracing was also conducted using MS analysis, and the setup is shown in Fig. S1b. All the deuterated samples in the experiment were used as received without further treatment. $CH_3OH$ and $H_2O$ (or their various deuterated counterparts) were first preheated separately to form individual vapors. These vapors were then mixed and introduced into a reactor containing the catalysts to initiate the coupling reaction. This procedure was designed to minimize the H–D exchange prior to the reaction. Bypass lines were designed to eliminate air intrusion during system installation. The molar ratios of $H_2$, HD and $D_2$ were obtained using previously calibrated sensitivity factors of 1, 0.73 and 0.73 for $H_2$, HD and $D_2$, respectively.

### 2.4 *In situ* infrared spectroscopy measurements

The *in situ* FT-IR test was carried out in the diffuse reflection mode, and the setup is shown in Fig. S2. The sample and KBr were mixed by grinding at a 1 : 100 mass ratio and loaded into the sample holder inside an Ar-filled glove box. During the test, the system was heated to the target temperature in an Ar atmosphere and maintained constant. After baseline correction of the solid sample, a $CH_3OH/H_2O$ mixed vapor was introduced to initiate the reaction. The spectra were collected every 5 minutes.

## 3. Results and discussions

### 3.1 Main mechanistic issues in MH-coupled MSR

MH-coupled MSR over $Cu/CaH_2$ can be written as follows (eqn (1)):

$$CaH_2 + CH_3OH + 2H_2O \rightarrow CaCO_3 + 5H_2 \quad (1)$$

In addition to providing $H_2$, the hydrolysis of hydride also generates heat to balance the endothermic MSR and captures $CO_2$ by the hydrolysis product $Ca(OH)_2$. There are three main mechanistic issues to be solved.

The first is whether the MH-coupled MSR is a synergetic reaction or a simple addition of three stepwise reactions: hydrolysis of $CaH_2$, MSR over Cu and $CO_2$ capture by $Ca(OH)_2$. The MH-coupled MSR involves hydrogen with different bonding natures: protonic hydrogen from –OH groups in water and methanol, covalent hydrogen from the $–CH_3$ group in methanol, and anionic hydrogen from $CaH_2$. How these hydrogen species with different bonding natures interact with each other is the second important mechanism issue. Finally, introducing $CaH_2$ into the MSR system might change the reaction pathway and the key intermediate during the $H_2$ generation. The third mechanism issue is the possible new reaction pathways and intermediates in MH-coupled MSR over Cu.

**3.1.1 Coupled reaction mechanism: synergetic or stepwise.** Online MS analysis was carried out to clarify whether the coupled reaction proceeded *via* a synergetic or stepwise pathway. MSR was carried out over Cu loaded on different supports with real-time monitoring of gaseous products using MS. The experimental conditions and results are summarized in Table S1 and Fig. 1a, respectively.

As shown in Fig. 1a, the hydrogen production of MSR over $Cu/CaH_2$ initiates within 2 min, which is within the residence time of the measurement system, indicating almost immediate $H_2$ generation. In contrast, MSR over $Cu/Ca(OH)_2$ and $Cu/Al_2O_3$

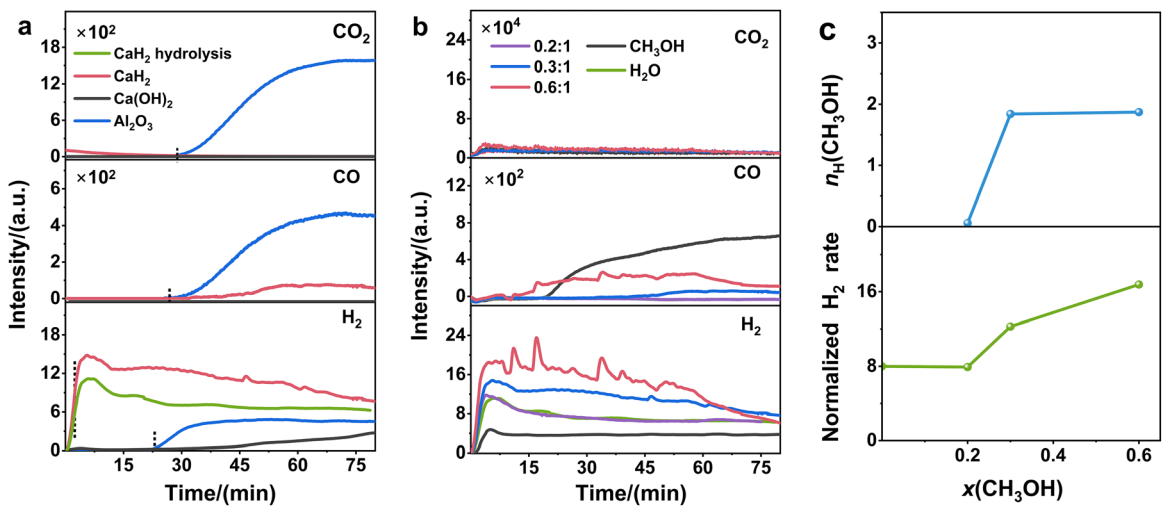


Fig. 1 Online MS profiles of (a) MSR over Cu supported on $CaH_2$, $Ca(OH)_2$ and $Al_2O_3$. Hydrolysis of $CaH_2$ is also included for comparison. (b) MSR over $Cu/CaH_2$ at different methanol-to-water molar ratios. (c) Time-averaged $H_2$ production rate in the first 40 min, and the corresponding number of hydrogen atoms released per methanol at different methanol-to-water molar ratios.

was notably slower, initiating around 43 and 20 minutes, respectively (Fig. S3). The initiation rate is similar for coupled MSR and direct hydrolysis over $Cu/CaH_2$ hydrolysis. However, the hydrogen generation rate is much faster for the coupled MSR. After 5 minutes, the peak signal was approximately 1.5 times higher. For comparison, the hydrogen generation rate of MSR over $Cu/Al_2O_3$ and $Cu/Ca(OH)_2$ reached only ~7% and ~3% of that over $Cu/CaH_2$, respectively (Fig. S3). In addition, in the first ~25 min, there is no detectable CO or $CO_2$ from the coupled MSR over $Cu/CaH_2$, as the generated $Ca(OH)_2$ effectively captures $CO_2$. Our previous study demonstrated that near-complete $CO_2$ capture was achieved when the generated $Ca(OH)_2$ was in excess, which agrees well with the online MS analysis.[33]

The impurities were observed in only the later stage of the coupled reaction when most of the $CaH_2$ was converted into $CaCO_3$. In contrast, a considerable amount of CO and $CO_2$ was detected by the MSR over Cu supported on $Al_2O_3$.

These results clearly demonstrate the advantages of coupled MSR over $Cu/CaH_2$ in terms of the hydrogen generation rate and $H_2$ purities. Moreover, the $Cu/CaH_2$ catalyst is significantly more reactive than the $Cu/Ca(OH)_2$, suggesting a synchronized reaction mechanism. The higher reactivity is attributed to the exothermicity from $CaH_2$ hydrolysis, which accelerates MSR kinetics.

Next, the effect of the methanol-to-water ratio was investigated to further clarify the contribution of MSR to hydrogen production in the coupled reaction by varying the methanol feed rate while keeping the water flow constant. Experimental conditions and results are presented in Table S2 and Fig. 1b and c.

As shown in Fig. 1b, introducing additional methanol clearly leads to a higher $H_2$ generation rate. Our previous study showed that the hydrolysis of $CaH_2$ proceeds nearly completely and much faster compared to MSR.[33] The additional $H_2$ generation over $Cu/CaH_2$ compared to that of $CaH_2$ hydrolysis is attributed to the coupled MSR process. To quantify the contribution of MSR to the $H_2$ generation, the $H_2$ signals from the first 40 minutes were integrated and averaged over time to give the time-averaged $H_2$ generation rate. As shown in Fig. 1c, the $H_2$ generation rate is 1.5 and 2.0 times higher than that of the hydrolysis reaction at $CH_3OH/H_2O$ molar ratios of 0.3 and 0.6, respectively. The number of hydrogen atoms contributed per methanol molecule was estimated using eqn (2):

$$n_H(CH_3OH) = [S_H(\text{total}) - S_H(H_2O)]/[x(CH_3OH)\cdot S_H(H_2O)], \quad (2)$$

where $S_H$(total) and $S_H(H_2O)$ are the integrated $H_2$ signals for methanol–water and water-only systems, respectively; and $x(CH_3OH)$ is the methanol-to-water molar ratio. As shown in Fig. 1c, $n_H(CH_3OH)$ is calculated to be around 1.84–1.87 when the methanol/water molar ratio is 0.3 and 0.6.

In $CH_3OH$, the –OH group is more acidic and can directly react with $CaH_2$ to produce $H_2$ and $(CH_3O)_2Ca$ (details discussed later), while the $–CH_3$ group is more inert. Our experiments show that methanol yields ~50% of the $H_2$ at the same molar feed rate of water (Fig. 1b), suggesting lower reactivity of the –OH group in methanol. Therefore, the more inert $–CH_3$ group must also be involved in the $H_2$ generation, contributing 0.8 (100% contribution of the –OH group, theoretically) ~1.3 (50% contribution of the –OH group from the experiment data) out of 3 hydrogen atoms. Despite uncertainties in MS quantification, these results highlight that the heat from $CaH_2$ hydrolysis effectively promotes C–H bond activation in methanol.

**3.1.2 Interactions among various hydrogen sources.** First, to clarify the role of hydridic H in $CaH_2$, a comparative study was conducted using $CaH_2$/KCl/Cu and Ca/KCl/Cu prepared *via* ball milling. Here, KCl is introduced to assist in the pulverization of large Ca granules into fine powder similar to that of $CaH_2$. Structural characterization by XRD and SEM (Fig. S4 and S5) suggests that the two samples have a similar structure. The hydrogen production performance of Ca/KCl/Cu and $CaH_2$/KCl/Cu coupled with MSR at 220 °C and a methanol-to-water molar ratio of 1 : 3 is shown in Fig. 2a (details are shown in Table S3). Both systems showed comparable results, with methanol conversions of ~66%, hydrogen purity above 99%, and only trace CO detected (0.10% and 0.16%). XRD analysis of the solid products (Fig. 2b) confirmed $CaCO_3$ formation in both samples, indicating that a coupling reaction occurred on both the Ca and $CaH_2$ surfaces. This was further supported by IR spectra (Fig. S6), which exhibited characteristic $CaCO_3$ peaks at 1440 and 876 $cm^{-1}$.[41]

Similar behaviors in coupled MSR on Ca and $CaH_2$ supported Cu catalysts indicate that the presence of $H^-$ in $CaH_2$ is not essential for the coupling process. If the reaction is exothermic and the hydrolysis products can capture $CO_2$, effective coupling can be achieved. This aligns with our previous findings on LiH and NaH.[34] Nevertheless, $CaH_2$ offers advantages over Ca, including a higher hydrogen yield density and a more moderate reaction heat.

To further probe the interactions among hydrogen species with different bonding natures, isotope tracing with online MS was employed to analyze isotope distribution in the evolved gas. The gas profiles and the time-averaged deuterium gas percentage $D_2$% are presented in Fig. 3.

It is interesting to note that when $CD_3OD/D_2O$ was fed to the system, notable $H_2$ formation is still observed (Fig. 3a), which can be tentatively attributed to the solid-state H exchange in the $CaH_2$–$Ca(OD)_2$ mixture (eqn (3)), as direct decomposition of $CaH_2$ requires a higher temperature:[42]

$$CaH_2 + Ca(OD)_2 = CaH_{2-x}D_x + Ca(OD)_{2-x}(OH)_x. \quad (3)$$

The H in $Ca(OD)_{2-x}(OH)_x$ is of a protonic nature and can combine with the hydridic H in $CaH_2$ directly to give $H_2$. Similarly, the apparent $D_2$ formation when feeding is $CH_3OD/H_2O$ and $CH_3OH/D_2O$ can also be explained by such solid-state H exchange.

Such complicated H exchange makes quantitative analysis of the contribution of each type of H very difficult. However, the different reactivity of H with different bonding natures can be

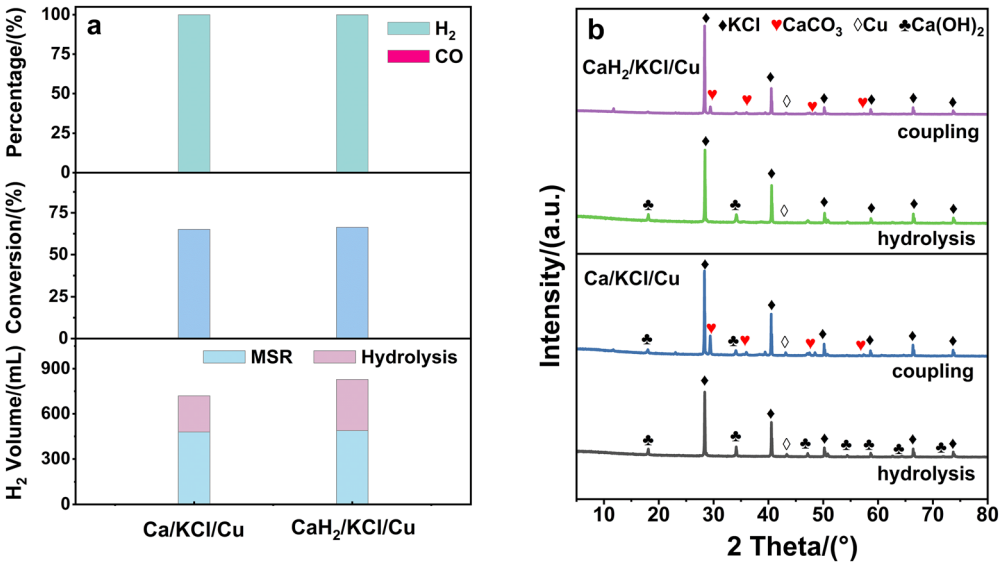


Fig. 2 Comparison of Ca/KCl/Cu and $CaH_2$/KCl/Cu coupled with MSR: (a) hydrogen yield, methanol conversion, and gas composition. (b) XRD patterns of the hydrolysis ($H_2O$) and coupling ($H_2O$ + $CH_3OH$) solid products.

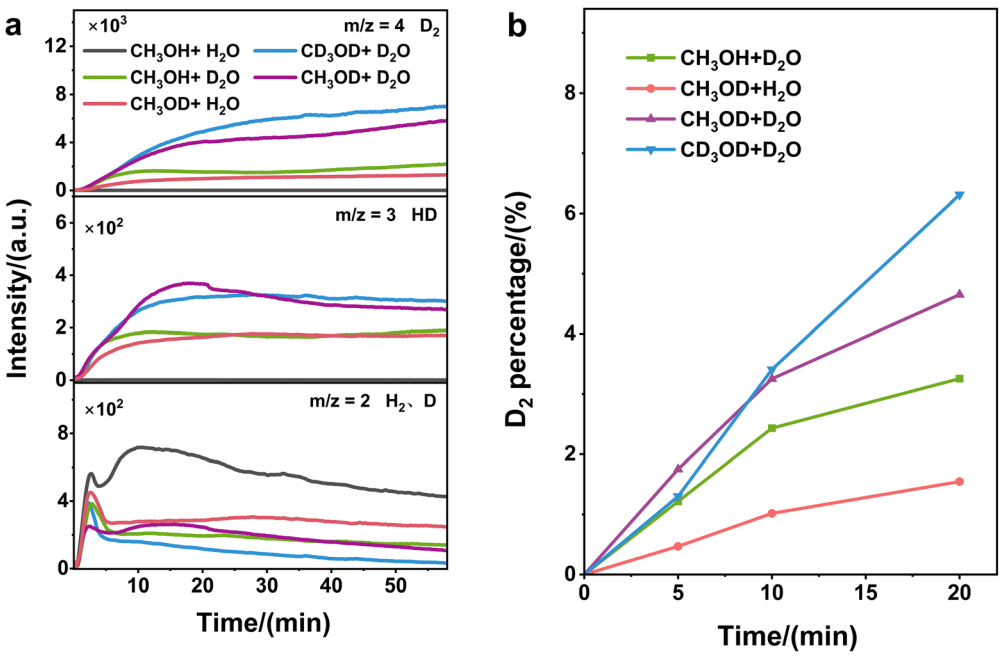


Fig. 3 (a) $H_2$, HD, and $D_2$ profiles of $CH_3OH$ and $H_2O$ over Cu/$CaH_2$ under different deuterium labelling conditions. (b) $D_2$ percentage in the evolved gas after different reaction times.

observed. The higher $D_2$% from $CH_3OH$–$D_2O$ compared to $CH_3OD$–$H_2O$ clearly indicates that H in $H_2O$ is more reactive compared to that in the –OH group of $CH_3OH$ (Fig. 3b). The peak that appeared at ~2 min in the $H_2$ signal after the feeding can be attributed to the rapid hydrolysis reaction (Fig. 3a).

Another interesting observation is that the $D_2$% in the first 5 min is even lower for $CD_3OD$/$D_2O$ compared to that of $CH_3OD$/$D_2O$ (Fig. 3b). This can be explained by the lower reactivity of the $-CH_3$ group in $CH_3OH$ overlapped with the kinetic isotope effect. However, the $D_2$% increases much more rapidly with time for $CD_3OD$/$D_2O$ compared to other D labelling precursors (Fig. 3b), indicating that D in the more stable $-CD_3$ group is released in the later stage of reaction. Compared to the peak of the $H_2$ signal at ~2 min, it can be concluded that the stable $-CD_3$ group was most likely activated by the heat from the hydrolysis of $CaH_2$.

**3.1.3 Identification of intermediates in the coupled reaction.** MSR on transition metals involves intermediates, such as methoxy ($-OCH_3$), formate ($HCOO^-$), formaldehyde (HCHO), and methyl formate ($HCOOCH_3$).[43–45] Introducing $CaH_2$ may

introduce new pathways and intermediates, potentially including calcium methoxide ($Ca(OCH_3)_2$) and calcium formate ($Ca(HCOO)_2$)—formed *via* reactions of $CaH_2$ with $CH_3OH$ and $HCOO^-$, respectively. The roles of these possible stable intermediates in the coupled reaction are first examined.

$Ca(OCH_3)_2$ can be formed by the direct reaction of $CaH_2$ and $CH_3OH$:

$$CaH_2 + 2CH_3OH \rightarrow Ca(OCH_3)_2 + 2H_2. \quad (4)$$

XRD analysis (Fig. S7) showed that $Ca(OCH_3)_2$ can be readily formed at 80 °C according to eqn (4) with or without Cu in an autoclave. The formed $Ca(OCH_3)_2$ remained unchanged within the temperature range of 80–250 °C, indicating its high thermal stability under reaction conditions. TPD–MS analysis (Fig. 4) revealed that $Ca(OCH_3)_2$ decomposes at ~530 °C to release $H_2$, and this temperature is unaffected when combined with $CaH_2$, CuO, or Cu/$CaH_2$. A weak $H_2$ signal at 310 °C in the Cu system was attributed to the desorption of pre-adsorbed hydrogen. These results further indicate that $Ca(OCH_3)_2$ is too stable to be an active intermediate for $H_2$ generation below 250 °C.

In the presence of $H_2O$, $Ca(OCH_3)_2$ can be converted into $CH_3OH$ and $Ca(OH)_2$ at 250 °C according to eqn (5).

$$Ca(OCH_3)_2 + 2H_2O \rightarrow Ca(OH)_2 + 2CH_3OH \quad (5)$$

$Ca(OH)_2$ and $CaCO_3$ are detected by XRD without and with a Cu catalyst (Fig. S8). Although $CH_3OH$ readily reacts with $CaH_2$ to form $Ca(OCH_3)_2$, the high thermal stability of $Ca(OCH_3)_2$ prevents further dehydrogenation under reaction conditions. The results suggest that despite its high thermal stability, $Ca(OCH_3)_2$, once formed, undergoes hydrolysis, which is expected to be significantly faster than thermal decomposition to regenerate $CH_3OH$ and return to conventional MSR mechanisms over Cu. In the coupled reaction, the generated $CO_2$ is absorbed by the $Ca(OH)_2$ from hydrolysis, yielding $CaCO_3$. Therefore, even if $Ca(OCH_3)_2$ is transiently formed, it is rapidly converted back to $CH_3OH$ and funneled into the main formate-mediated MSR pathway.

Then, another possible stable intermediate, $Ca(HCOO)_2$, was investigated, which may be formed from the following reaction (eqn (6)):

$$CaH_2 + 2HCOOH = Ca(HCOO)_2 + H_2. \quad (6)$$

These results suggest that $CaH_2$ readily reacts with HCOOH to form $Ca(HCOO)_2$, as confirmed by the XRD results (Fig. S9). Similar to $Ca(OCH_3)_2$, $Ca(HCOO)_2$ also exhibits high thermal stability. The decomposition temperature is ~450 °C. By mixing with $Ca(OH)_2$ and $Ca(OH)_2$/CuO, the decomposition temperature is only slightly reduced to ~410 °C, suggesting that $Ca(HCOO)_2$ is not a key intermediate for the $H_2$ generation in the coupled MSR either (Fig. 5). Considering that the decomposition temperature of $Ca(HCOO)_2$ is far higher than the reaction temperature employed in this study, its thermal decomposition is unlikely to occur under reaction conditions. Instead, any transiently formed $Ca(HCOO)_2$ would be rapidly converted back to formate-related intermediates in the presence of $H_2O$, thereby allowing the reaction to proceed through the conventional formate-mediated MSR pathway.

After excluding these stable intermediates, we further examined the unstable intermediates using *in situ* diffuse reflectance infrared Fourier transform spectroscopy (DRIFTS). The main species of interest and the characteristic peaks of their corresponding functional groups[43–45] are listed in Table S4.

Fig. 6 and Fig. S10 summarize the *in situ* DRIFTS spectra of MSR over Cu/$CaH_2$ and Cu/$Al_2O_3$ from 100 to 250 °C. The peaks at 1032 and 1057 $cm^{-1}$ are related to adsorbed $CH_3OH$. The key intermediates are formate species, as evidenced by the 1580–1600 and 1367–1376 $cm^{-1}$ peaks.[46,47] On Cu/$CaH_2$, peaks corresponding to formate[48] (1597 and 1371 $cm^{-1}$) readily appeared even at 100 °C after introducing the $CH_3OH$–$H_2O$ mixture for only 10 min (Fig. 6a), implying initiation of the coupled MSR at a very mild temperature. These peaks intensified at higher temperatures (Fig. 6a–c). In contrast, only $CH_3OH$-related peaks from the adsorbed $CH_3OH$ were observed on the Cu/$Al_2O_3$ surface at 100 °C (Fig. 6a). $HCOO^-$-related peaks only began

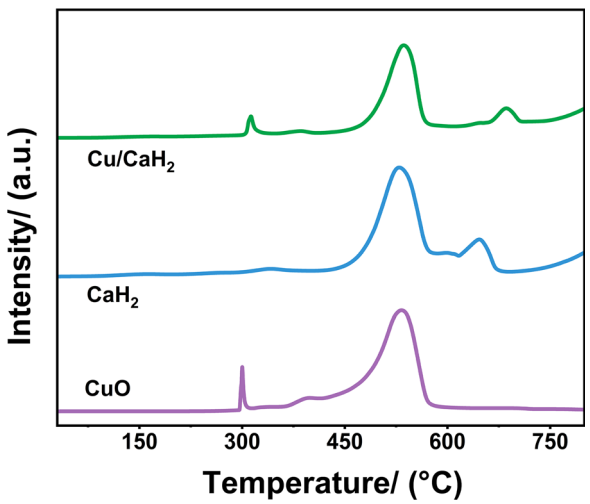


Fig. 4 TPD–MS $H_2$ signals for $Ca(OCH_3)_2$ containing CuO, $CaH_2$ or Cu/$CaH_2$.

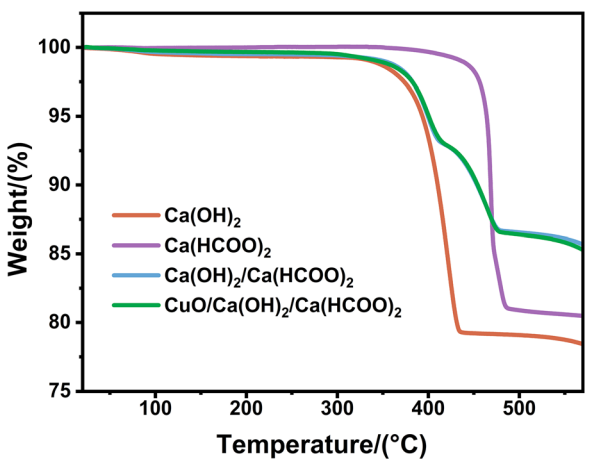


Fig. 5 Thermogravimetric profiles of the $Ca(HCOO)_2$-containing samples.

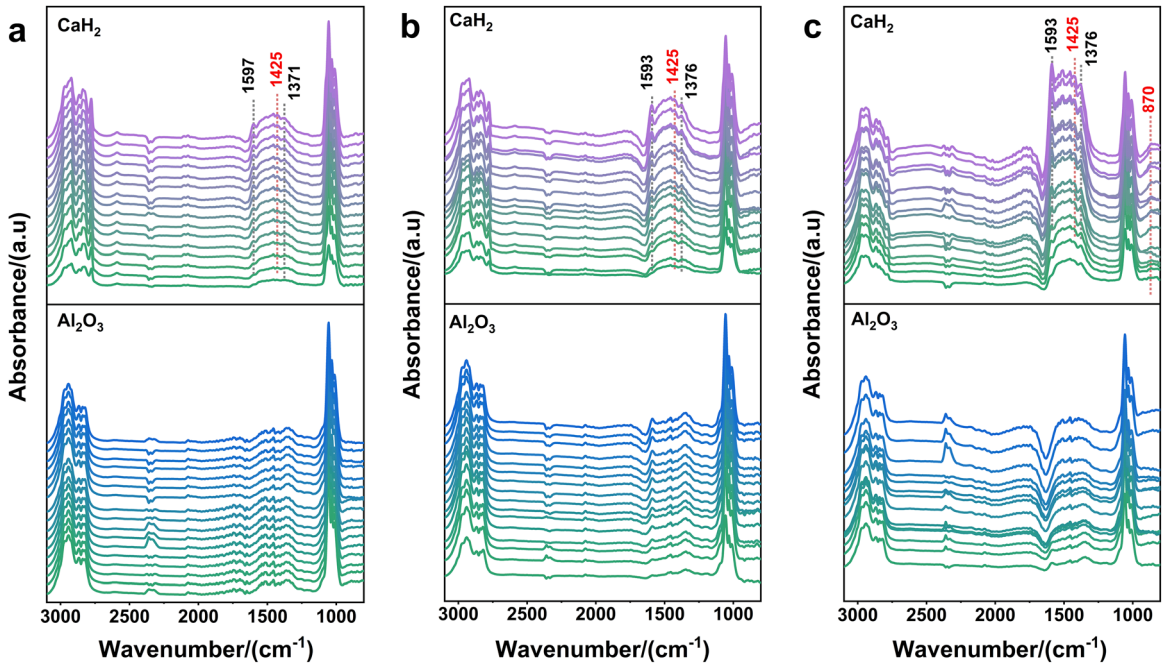


Fig. 6 *In situ* DRIFT spectra obtained after the reaction of $Cu/Al_2O_3$ and $Cu/CaH_2$ with the $CH_3OH/H_2O$ mixed vapor (molar ratio 1 : 3) at different temperatures: (a) 100 °C, (b) 150 °C, and (c) 200 °C.

to emerge at 150 °C (Fig. 6b). Peaks corresponding to fully dehydrogenated products $CO_2$ (2360 $cm^{-1}$) and CO (2181 $cm^{-1}$) were only detected above 200 °C and become prominent only at 250 °C (Fig. S10), suggesting that effective MSR over $Cu/Al_2O_3$ requires high temperature.

The formate-related peaks are much weaker over $Cu/Al_2O_3$. On $Cu/Al_2O_3$ at 250 °C (Fig. S10), there is a clear $CO_2$-related peak at 2360 $cm^{-1}$ and CO (2178 $cm^{-1}$),[46] which increases over time. In contrast, no clear $CO_2$ or CO peaks were observed on $Cu/CaH_2$ (Fig. S10). Instead, carbonate-related peaks at 1425 and 870 $cm^{-1}$ (ref. 41) are detected, which suggests effective $CO_2$ capture in the MH-coupled MSR.

To investigate the intermediate evolution during the coupled reaction, temporal changes in methoxy and formate peak intensities over $Cu/CaH_2$ were monitored after stopping the $CH_3OH$ and $H_2O$ feed (Fig. 7a). As shown in Fig. 7b, the methoxy-related peak at 1030 $cm^{-1}$ decreased whereas the formate-related peak at 1585 $cm^{-1}$ increased, indicating a methoxy-to-formate transformation pathway.

The *in situ* FT-IR results suggest that the MH-coupled MSR over $Cu/CaH_2$ also proceeds *via* the $HCOO^-$ intermediate, which is the same as on conventional Cu catalysts. However, the presence of MH facilitates MSR initiation, promotes formate formation, and accelerates its decomposition at much lower temperatures (~100 °C) due to localized heat and alkaline conditions from $CaH_2$ hydrolysis. These results are in agreement with the hydrogen generation and online MS data.

### 3.2 Proposed mechanism for the coupled reaction

Based on the above experimental results, we propose the mechanism of MSR-coupled hydrogen production over the $Cu/CaH_2$ system, as illustrated in Fig. 8.

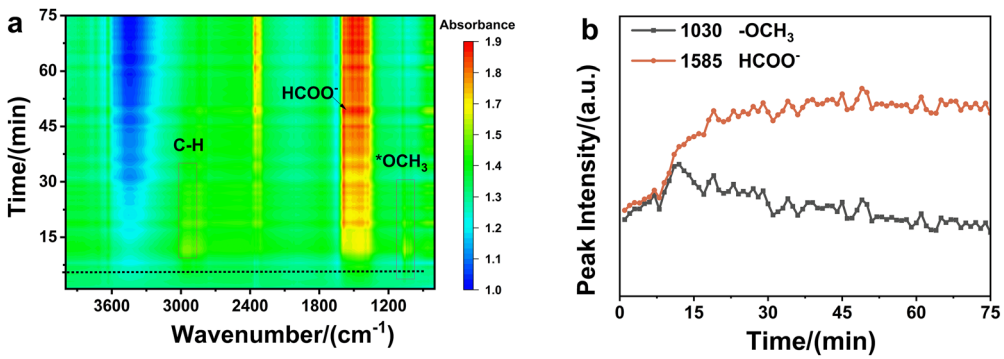


Fig. 7 (a) Time-dependent DRIFTS spectra of MSR and (b) peak intensity of methoxy at 1030 $cm^{-1}$ and formate at 1585 $cm^{-1}$ over $Cu/CaH_2$. The $CH_3OH/H_2O$ mixed vapor (molar ratio-1 : 3) was introduced into the chamber for 10 min.

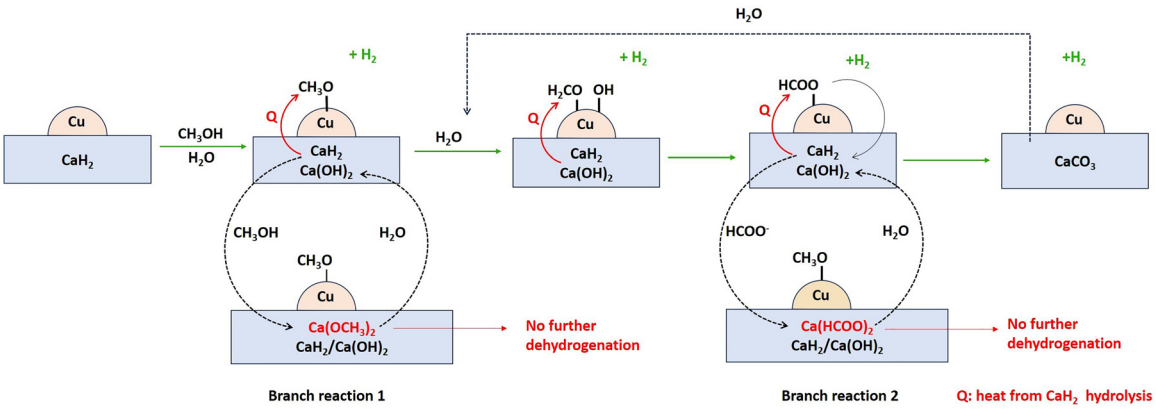


Fig. 8 Schematic of the coupled reaction mechanism.

The main evolution pathway of $CH_3OH$ over Cu follows the conventional $HCOO^-$ pathway. The MH plays two important roles: (1) supplying heat to initiate MSR, particularly endothermic C–H bond dissociation, at a lower temperature, and accelerating their conversion to $CO_2$; (2) $Ca(OH)_2$ captures $CO_2$, which also facilitates the water–gas shift reaction and suppresses CO formation.

$CaH_2$ introduces two possible new intermediates: $Ca(OCH_3)_2$ from the direct reaction of $CH_3OH$ with $CaH_2$, and $Ca(HCOO)_2$ from the reaction of HCOOH with $CaH_2$. However, both species are highly thermally stable and cannot directly release hydrogen. In the presence of water, however, they can be hydrolyzed to regenerate $CH_3OH$ and $HCOO^-$ adsorbed on the Cu surface, re-entering the main reaction pathway, as shown in the two branch reactions of Fig. 8.

## 4. Conclusions

This study provides a systematic study on the mechanism of hydrogen production from MH-coupled methanol steam reforming (MSR) on the $Cu/CaH_2$ system. The main conclusions are as follows.

(1) The MH-coupled MSR proceeds *via* a synergetic mechanism instead of the simple addition of separated MSR over Cu and hydrolysis of $CaH_2$ and $CO_2$ capture by $Ca(OH)_2$. Online MS analysis suggests that $CH_3OH$ starts to release $H_2$ in the initial stage of the reaction from both the hydroxyl and methyl groups in the molecule, which is concomitant with the hydrolysis of $CaH_2$.

(2) Isotope labelling study suggests a complicated exchange of H with different bonding natures. The hydridic H in $CaH_2$ is not essential for synergized MSR, while $CaH_2$ is superior to Ca owing to its higher H density and milder thermal effect.

(3) The evolution of $CH_3OH$ over Cu follows the conventional $HCOO^-$ pathway. The MH provides heat to facilitate the MSR at lower temperatures and eliminate both $CO_2$ and CO. $Ca(OCH_3)_2$, and $Ca(HCOO)_2$ might be formed in the synergized MSR process, while they are not active intermediates for hydrogen generation at mild temperatures due to their high thermal stability. These intermediates, once formed, can react with water, regenerate $CH_3OH$ and HCOOH and return to the main reaction mechanism.

## Conflicts of interest

There are no conflicts to declare.

## Data availability

The data supporting this study are available within the article and its supplementary information (SI). Supplementary information is available. This supplementary information document provides comprehensive experimental details, material characterizations, and mechanistic insights supporting this study. It includes detailed schematics of the online MS and *in situ* IR setups, alongside tables outlining specific reaction conditions. Furthermore, the document presents XRD and SEM-EDS characterizations to confirm the physical and chemical properties of the synthesized catalysts. Finally, it provides quantitative data on hydrogen yield and gas composition, coupled with *in situ* DRIFTS and IR spectral analyses, to elucidate the reaction intermediates and the underlying hydrogen production pathways. See DOI: https://doi.org/10.1039/d6ey00038j.

## Acknowledgements

This work is supported by the MOST of China (No. 2024YFE0207400), NSFC (No. 22579003) and the Key Project of Jiangsu Province Basic Research Program (No. BK20243033).

## References

1 K. T. Møller, T. R. Jensen, E. Akiba and H. Li, Hydrogen – A sustainable energy carrier, *Prog. Nat. Sci.: Mater. Int.*, 2017, **27**, 34–40.
2 L. Zhang, C. Jia, F. Bai, W. Wang, S. An, K. Zhao, Z. Li, J. Li and H. Sun, A comprehensive review of the promising clean energy carrier: hydrogen production, transportation,

storage, and utilization (HPTSU) technologies, *Fuel*, 2024, **355**, 129455.
3 J. O. Abe, A. P. I. Popoola, E. Ajenifuja and O. M. Popoola, Hydrogen energy, economy and storage: review and recommendation, *Int. J. Hydrogen Energy*, 2019, **44**, 15072–15086.
4 A. Züttel, Hydrogen storage methods, *Naturwissenschaften*, 2004, **91**, 157–172.
5 M. R. Usman, Hydrogen storage methods: review and current status, *Renewable Sustainable Energy Rev.*, 2022, **167**, 112743.
6 H. Barthélémy, M. Weber and F. Barbier, Hydrogen storage: recent improvements and industrial perspectives, *Int. J. Hydrogen Energy*, 2017, **42**, 7254–7262.
7 K. Kappis, J. Papavasiliou and G. Avgouropoulos, Methanol reforming processes for fuel cell applications, *Energies*, 2021, **14**, 8442.
8 L. Ouyang, M. Liu, K. Chen, J. Liu, H. Wang, M. Zhu and V. Yartys, Recent progress on hydrogen generation from the hydrolysis of light metals and hydrides, *J. Alloys Compd.*, 2022, **910**, 164831.
9 D. Jifeng, C. Shunpeng, W. Xiaojuan, Z. Jie and L. Xingguo, Recent progress on materials for hydrogen generation *via* hydrolysis, *J. Inorg. Mater.*, 2021, **36**, 1.
10 B. Hu, R. Shu, Z. Tian, C. Wang, Y. Chen and Y. Xu, Enhancement of hydrogen production *via* methanol steam reforming using a Ni-based catalyst supported by spongy mesoporous alumina, *Green Chem.*, 2024, **26**, 5485–5498.
11 R. Shu, L. Xie, B. Hu, Z. Tian, C. Wang, Y. Chen and Y. Xu, Reinforcement of methanol catalytic reforming for hydrogen production through Ru-based carbon-coated $CeO_2$ catalyst, *Fuel*, 2024, **365**, 131262.
12 D. R. Palo, R. A. Dagle and J. D. Holladay, Methanol steam reforming for hydrogen production, *Chem. Rev.*, 2007, **107**, 3992–4021.
13 A. H. Mohammed Abbas, K. K. Cheralathan, E. Porpatham and S. K. Arumugam, Hydrogen generation using methanol steam reforming – catalysts, reactors, and thermo-chemical recuperation, *Renewable Sustainable Energy Rev.*, 2024, **191**, 114147.
14 M. Usman and T. Yamada, Methanol reforming for hydrogen production: advances in catalysts, nanomaterials, reactor design, and fuel cell integration, *ACS Eng. Au*, 2025, **5**, 314–346.
15 H. Meng, Y. Yang, T. Shen, Z. Yin, L. Wang, W. Liu, P. Yin, Z. Ren, L. Zheng and J. Zhang, Designing $Cu^0$–$Cu^+$ dual sites for improved C–H bond fracture towards methanol steam reforming, *Nat. Commun.*, 2023, **14**, 7980.
16 K. Ploner, P. D. K. Nezhad, M. Watschinger, L. Schlicker, M. F. Bekheet, A. Gurlo, A. Gili, A. Doran, S. Schwarz and M. Stöger-Pollach, Steering the methanol steam reforming performance of $Cu/ZrO_2$ catalysts by modification of the Cu–$ZrO_2$ interface dimensions resulting from Cu loading variation, *Appl. Catal., A*, 2021, **623**, 118279.
17 M. Kusche, F. Enzenberger, S. Bajus, H. Niedermeyer, A. Bösmann, A. Kaftan, M. Laurin, J. Libuda and P. Wasserscheid, Enhanced activity and selectivity in catalytic methanol steam reforming by basic alkali metal salt coatings, *Angew. Chem., Int. Ed.*, 2013, **52**, 5028–5032.
18 L. Xie, B. Hu, R. Shu, Z. Tian, Y. Chen and C. Wang, Effect of oxygen vacancy influenced by $CeO_2$ morphology on the methanol catalytic reforming for hydrogen production, *Int. J. Hydrogen Energy*, 2023, **48**, 33119–33129.
19 H. Li, H. Tian, S. Chen, Z. Sun, T. Liu, R. Liu, S. Assabumrungrat, J. Saupsor, R. Mu, C. Pei and J. Gong, Sorption enhanced steam reforming of methanol for high-purity hydrogen production over Cu–$MgO/Al_2O_3$ bifunctional catalysts, *Appl. Catal., B*, 2020, **276**, 119052.
20 Q. Liu, S. Du, T. Liu, L. Gong, Y. Wu, J. Lin, P. Yang, G. Huang, M. Li, Y. Wu, Y. Zhou, Y. Li, L. Tao and S. Wang, Efficient low-temperature hydrogen production by electrochemical-assisted methanol steam reforming, *Angew. Chem.*, 2024, **136**, e202315157.
21 S. T. Yong, C. W. Ooi, S. P. Chai and X. S. Wu, Review of methanol reforming – Cu-based catalysts, surface reaction mechanisms, and reaction schemes, *Int. J. Hydrogen Energy*, 2013, **38**, 9541–9552.
22 D. Li, F. Xu, X. Tang, S. Dai, T. Pu, X. Liu, P. Tian, F. Xuan, Z. Xu, I. E. Wachs and M. Zhu, Induced activation of the commercial $Cu/ZnO/Al_2O_3$ catalyst for the steam reforming of methanol, *Nat. Catal.*, 2022, **5**, 99–108.
23 J. L. C. Fajín and M. N. D. S. Cordeiro, Insights into the mechanism of methanol steam reforming for hydrogen production over Ni–Cu-based catalysts, *ACS Catal.*, 2022, **12**, 512–526.
24 C. J. Jiang, D. L. Trimm, M. S. Wainwright and N. W. Cant, Kinetic mechanism for the reaction between methanol and water over a Cu–ZnO–$Al_2O_3$ catalyst, *Appl. Catal., A*, 1993, **97**, 145–158.
25 L. Jiang, S. Yuan, J. Ma, S. Deng, X. Fang, X. Xu, H. Meng and X. Wang, Enhancing the reactivity of $Cu/Al_2O_3$ for methanol steam reforming through adding CrOx: unraveling reaction pathways and the mechanism for improvement, *ACS Catal.*, 2025, **15**, 7138–7152.
26 X. Tang, Y. Wu, Z. Fang, X. Dong, Z. Du, B. Deng, C. Sun, F. Zhou, X. Qiao and X. Li, Syntheses, catalytic performances and DFT investigations: a recent review of copper-based catalysts of methanol steam reforming for hydrogen production, *Energy*, 2024, 131091.
27 N. Takezawa and N. Iwasa, Steam reforming and dehydrogenation of methanol: difference in the catalytic functions of copper and group VIII metals, *Catal. Today*, 1997, **36**, 45–56.
28 A. A. Lytkina, N. A. Zhilyaeva, M. M. Ermilova, N. V. Orekhova and A. B. Yaroslavtsev, Influence of the support structure and composition of Ni–Cu-based catalysts on hydrogen production by methanol steam reforming, *Int. J. Hydrogen Energy*, 2015, **40**, 9677–9684.
29 H. Wang, Z. Fang, Y. Wang, K. Meng and S. Sun, The study of strong metal–support interaction enhanced PdZn alloy nanocatalysts for methanol steam reforming, *J. Alloys Compd.*, 2024, **986**, 174006.
30 M. A. Diaz-Perez, J. Moya, J. C. Serrano-Ruiz and J. Faria, Interplay of support chemistry and reaction conditions on

copper catalyzed methanol steam reforming, *Ind. Eng. Chem. Res.*, 2018, **57**, 10285–10294.
31 L. Zhang, L. Pan, C. Ni, T. Sun, S. Zhao, S. Wang, A. Wang and Y. Hu, $CeO_2$–$ZrO^2$-promoted CuO/ZnO catalyst for methanol steam reforming, *Int. J. Hydrogen Energy*, 2013, **38**, 4397–4406.
32 X. Min, D. Chai, K. Ding, R. Li and X. Zhang, Hydrogen generation by hydrolysis of solid sodium borohydride for portable PEMFC applications, *Fuel*, 2023, **350**, 128777.
33 K. Kadeer, X. Li and J. Zheng, Hydrogen generation by coupling methanol steam reforming with metal hydride hydrolysis, *Chem. Commun.*, 2023, **59**, 5443–5446.
34 K. Kadeer, Y. Jiang, Y. Huang, Y. Lin, R. Jin, C. Yin, F. Guo, T. Ichikawa, X. Li and J. Zheng, Hydrogen generation from coupled methanol steam reforming with metal hydride hydrolysis: effects of metal catalysts and hydrides, *Int. J. Hydrogen Energy*, 2025, **102**, 29–36.
35 L. Ouyang, M. Liu, K. Chen, J. Liu, H. Wang, M. Zhu and V. Yartys, Recent progress on hydrogen generation from the hydrolysis of light metals and hydrides, *J. Alloys Compd.*, 2022, **910**, 164831.
36 Y. Wu, Y. Guo, H. Yu, X. Jiang, Y. Zhang, Y. Qi, K. Fu, L. Xie, G. Li, J. Zheng and X. Li, Nonstoichiometric yttrium hydride–promoted reversible hydrogen storage in a liquid organic hydrogen carrier, *CCS Chem.*, 2020, **3**, 974–984.
37 H. Yu, X. Li and J. Zheng, Beyond hydrogen storage: metal hydrides for catalysis, *ACS Catal.*, 2024, **14**, 3139–3157.
38 M. S. Salman, N. Rambhujun, C. Pratthana, K. Srivastava and K.-F. Aguey-Zinsou, Catalysis in liquid organic hydrogen storage: recent advances, challenges, and perspectives, *Ind. Eng. Chem. Res.*, 2022, **61**, 6067–6105.
39 X. Jiang, X. Nie, X. Guo, C. Song and J. G. Chen, Recent advances in carbon dioxide hydrogenation to methanol *via* heterogeneous catalysis, *Chem. Rev.*, 2020, **120**, 7984–8034.
40 P. Wang, F. Chang, W. Gao, J. Guo, G. Wu, T. He and P. Chen, Breaking scaling relations to achieve low-temperature ammonia synthesis through LiH-mediated nitrogen transfer and hydrogenation, *Nat. Chem.*, 2017, **9**, 64–70.
41 S. Gunasekaran, G. Anbalagan and S. Pandi, Raman and infrared spectra of carbonates of calcite structure, *J. Raman Spectrosc.*, 2006, **37**, 892–899.
42 S. Balakrishnan, T. D. Humphries, M. Paskevicius and C. E. Buckley, Thermodynamic and kinetic properties of calcium hydride, *Int. J. Hydrogen Energy*, 2023, **48**, 30479–30488.
43 D. Li, X. Li and J. Gong, Catalytic reforming of oxygenates: state of the art and future prospects, *Chem. Rev.*, 2016, **116**, 11529–11653.
44 S. Lin, D. Xie and H. Guo, Methyl formate pathway in methanol steam reforming on copper: density functional calculations, *ACS Catal.*, 2011, **1**, 1263–1271.
45 S. T. Yong, C. W. Ooi, S. P. Chai and X. S. Wu, Review of methanol reforming—Cu-based catalysts, surface reaction mechanisms, and reaction schemes, *Int. J. Hydrogen Energy*, 2013, **38**, 9541–9552.
46 H. Meng, Y. Yang, T. Shen, Z. Yin, L. Wang, W. Liu, P. Yin, Z. Ren, L. Zheng, J. Zhang, F.-S. Xiao and M. Wei, Designing $Cu^0$–$Cu^+$ dual sites for improved C–H bond fracture towards methanol steam reforming, *Nat. Commun.*, 2023, **14**, 7980.
47 S. D. Lin, H. Cheng and T. C. Hsiao, *In situ* DRIFTS study on the methanol oxidation by lattice oxygen over Cu/ZnO catalyst, *J. Mol. Catal. A: Chem.*, 2011, **342–343**, 35–40.
48 L. F. Bobadilla, L. Azancot, S. Ivanova, J. J. Delgado, F. Romero-Sarria, M. A. Centeno, A.-C. Roger and J. A. Odriozola, *In situ* DRIFTS-MS methanol adsorption study onto supported NiSn nanoparticles: mechanistic implications in methanol steam reforming, *Nanomaterials*, 2021, **11**, 3234.